Supplemental Material

Universality of Anderson Localization Transitions in the Integer and Fractional Quantum Hall Regime

Simrandeep Kaur[†1], Tanima Chanda[†1], Kazi Rafsanjani Amin[†2], Kenji Watanabe[3], Takashi Taniguchi[4], Unmesh Ghorai[5], Yuval Gefen[6], G. J. Sreejith[7] and Aveek Bid[1*]

[1]*Department of Physics, Indian Institute of Science, Bangalore 560012, India.*

[2]*Department of Microtechnology and Nanoscience, Chalmers University of Technology, 412 96 Gothenburg, Sweden.*

[3]*Research Center for Electronic and Optical Materials, National Institute for Materials Science, 1-1 Namiki, Tsukuba 305-0044, Japan.*

[4]*Research Center for Materials Nanoarchitectonics, National Institute for Materials Science, 1-1 Namiki, Tsukuba 305-0044, Japan.*

[5]*Department of Theoretical Physics, Tata Institute of Fundamental Research, Homi Bhabha Road, Mumbai, 400005, India*

[6] *Department of Condensed Matter Physics, Weizmann Institute of Science, Rehovot 76100, Israel.*

[7]*Indian Institute of Science Education and Research, Pune 411008, India.*

CONTENTS

S1. Device fabrication, schematics and characterization 3

S2. Estimation of κ from the temperature dependence of the width of R_{xx}. 4

S3. Critical behavior of various plateau-to-plateau transitions 5

S4. The scaling behavior of Quantum Hall states in low-mobility devices 5

S5. Second derivative of R_{xy} with temperature. 6

S6. Fractional Quantum Hall states at $B = 4.5$ T. 7

S7. Details of scaling analysis. 8

S8. Values of κ from previous studies 9

References 18

* aveek@iisc.ac.in

S1. DEVICE FABRICATION, SCHEMATICS AND CHARACTERIZATION

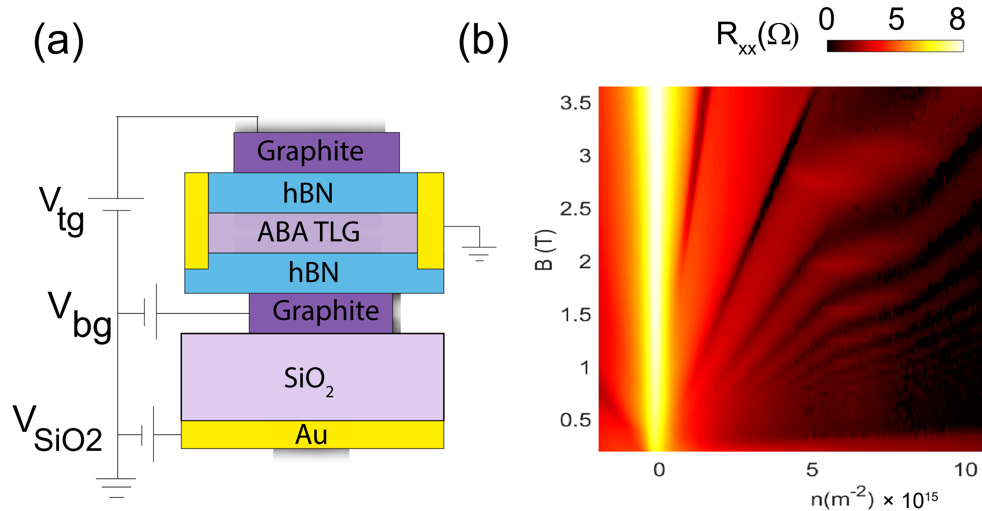

FIG. S1. (a) Schematic of the device. Two gates V_{bg} and V_{tg} (with 30 nm thick hBN flakes as gate dielectrics and thin graphite as gate contacts) are used to tune the number density and displacement field across the flake. A silicon back-gate (with SiO_2 as the gate dielectric) is used to dope the graphene contacts of the device to prevent the formation of p-n junctions. (b) Landau level fan diagram for TLG measured at 7 K. Color map shows the R_{xx} in log scale.

Bernal-stacked trilayer graphene (TLG), hBN, and graphite flakes are mechanically exfoliated on Si substrates with a 300 nm thick top SiO_2 layer. TLG flakes are first identified through color contrast under an optical microscope and further confirmed using Raman spectroscopy [1, 2]. The standard dry pickup and transfer technique is used to fabricate the heterostructure. The flakes are picked up sequentially using polycarbonate (PC) film at $T = 120^\circ$ C in the following order: graphite/hBN/TLG/hBN/graphite. The entire stack, along with the PC film, is transferred on Si/SiO_2 substrate at 180° C followed by cleaning in chloroform, acetone, and IPA solution to remove the PC residue. The heterostructure is then annealed in vacuum at 300° C for 4 hours. We employ electron beam lithography for defining the contacts on the heterostructure. This is followed by etching with a mixture of CHF_3 and O_2 gases and metal deposition with Cr/Pd/Au (3 nm/12 nm/55 nm) to create 1-D contacts [3, 4].

Avoiding the formation of p-n junctions is absolutely essential if the devices are to be operated

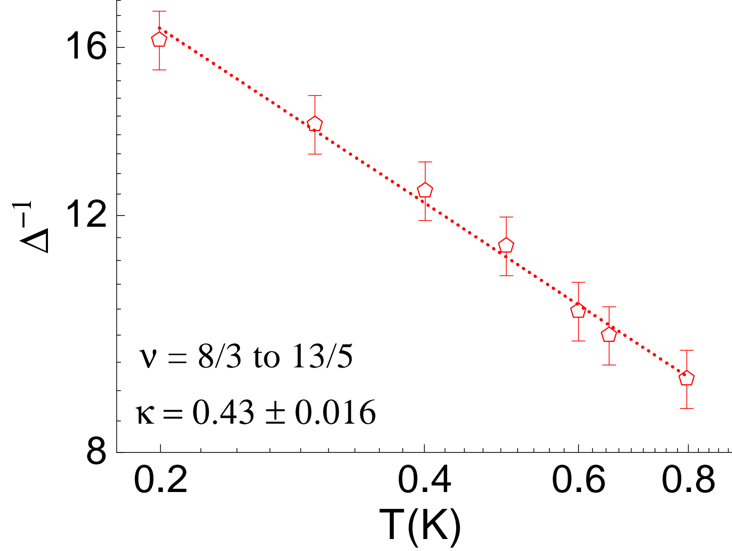

FIG. S2. **Calculating κ from width of R_{xx}.** Log-log plots of the inverse of the half-width of longitudinal magnetoresistance R_{xx} versus T for PT between $\nu = 2 + 2/3$ and $\nu = 2 + 3/5$.

at high displacement fields [5–7]. We achieve this by doping the graphene contacts (that extend out of both the graphite gates) to high charge-carrier density. A schematic of the device is shown in Fig. S1(a). Two common kinds of TLG flakes are typically obtained during mechanical exfoliation: ABA (or Bernal-stacked) and ABC. ABC, being a metastable stacking [8, 9], generally converts into ABA stacking during fabrication. These two phases are easily distinguishable by Raman spectroscopy and transport measurements – displacement field opens up a band gap in ABC TLG [10–12]. In contrast, a band gap does not open in ABA TLG.

Fig. S1(b) shows the Landau level fan diagram of the sample measured at 7 K. It matches pretty well with the simulated LL plot shown in Fig. 1(d) of the main manuscript with clear indications of monolayer-like Landau levels (LL) around a charge-carrier density 5×10^{15} m^{-2} that cross the bilayer-like LLs confirming the system to be ABA trilayer graphene [13, 14].

S2. ESTIMATION OF κ FROM THE TEMPERATURE DEPENDENCE OF THE WIDTH OF R_{xx}.

At the critical point of the quantum Hall plateau-to-plateau transitions (PT), both dR_{xy}/dν and the inverse of the half-width of R_{xx} versus ν plot diverge according to power law $T^{-\kappa}$ [15]. In the main manuscript, we estimated the value of κ by evaluating dR_{xy}/dν close to the critical point. Here, we focus on the analysis of the width Δ of R_{xx} (FWHM of R_{xx} transition peak) versus ν

[16, 17]. At the critical point, Δ^{-1} diverges like $T^{-\kappa}$. The dependence of Δ^{-1} on T for the transition between $\nu = 2 + 2/3$ and $\nu = 2 + 3/5$ is shown in Fig. S2. The slope of linear fits to data yields $\kappa = 0.43 \pm 0.016$.

S3. CRITICAL BEHAVIOR OF VARIOUS PLATEAU-TO-PLATEAU TRANSITIONS

In table S1, we compare our experimentally obtained values of ν_c with the theoretically predicted values [18, 19]:

$$\nu_c = \frac{(n + 0.5)}{2\,(n + 0.5) \pm 1}; \tag{S1}$$

where n is the LL index of composite Fermions.

ν_1	ν_2	ν_c^{xy}	ν_c^{xx}	ν_c (predicted)
$\nu = \frac{7}{3}$	$\nu = \frac{12}{5}$	2.375 ± 0.002	2.371 ± 0.003	2.375
$\nu = \frac{12}{5}$	$\nu = \frac{17}{7}$	–	2.417 ± 0.003	2.417
$\nu = \frac{18}{7}$	$\nu = \frac{13}{5}$	–	2.586 ± 0.002	2.583
$\nu = \frac{13}{5}$	$\nu = \frac{8}{3}$	2.625 ± 0.003	2.624 ± 0.002	2.625
$\nu = \frac{10}{3}$	$\nu = \frac{17}{5}$	3.377 ± 0.002	3.371 ± 0.003	3.375
$\nu = \frac{17}{5}$	$\nu = \frac{24}{7}$	3.416 ± 0.003	3.417 ± 0.003	3.417
$\nu = \frac{25}{7}$	$\nu = \frac{18}{5}$	–	3.588 ± 0.002	3.583
$\nu = \frac{18}{5}$	$\nu = \frac{11}{3}$	–	3.624 ± 0.004	3.625

TABLE S1. Experimentally determined values of ν_c for high-mobility Bernal-stacked trilayer graphene devices for plateau-to-plateau transition between filling factors ν_1 and ν_2. ν_c^{xy} (ν_c^{xx}) is the value of the critical filling factor obtained from the crossing points of R_{xy} (maxima of R_{xx}). Also tabulated are the theoretical predictions for ν_c [18, 19].

S4. THE SCALING BEHAVIOR OF QUANTUM HALL STATES IN LOW-MOBILITY DEVICES

To compare the effect of long-range and short-range potential disorders [20] on the scaling exponents, we fabricated hBN-encapsulated graphene heterostructures without the back graphite electrode. The number density across these devices is tuned using a Si/SiO_2 gate. Despite being hBN encapsulated, effects of Coulomb impurities present at the SiO_2 surface containing dangling

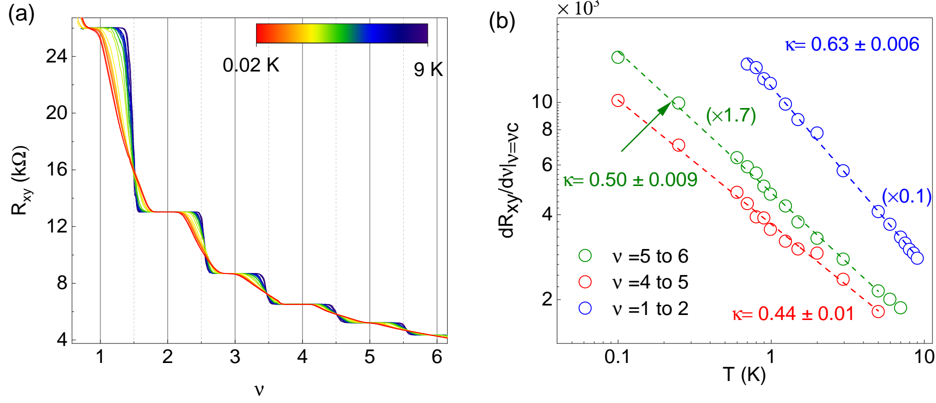

FIG. S3. **Scaling exponents in low mobility graphene device**.(a) Plots of R_{xy} versus filling factor at different temperatures. (b) Plots of $\mathrm{d}R_{xy}/\mathrm{d}\nu$ at the critical point $\nu = \nu_C$ versus temperature (log-log scale) for various plateau-to-plateau transitions. The values of κ extracted from the plots are mentioned in the plot.

bonds are not screened. These lead to long-range potential fluctuations across the device [21, 22]. Fig. S3 shows the variation of $\mathrm{d}R_{xy}/\mathrm{d}\nu$ at $\nu = \nu_c$ as a function of temperature for one such device for different plateau-to-plateau transitions. We observe a large spread in values of the scaling exponent κ, as opposed to the case of high-mobility devices discussed in the main manuscript, where the values of κ were tightly clustered around the theoretically predicted value of 0.42. Our analysis supports the recent observations where the presence of long-range interactions made the scaling exponent non-universal [23].

S5. SECOND DERIVATIVE OF R_{xy} WITH TEMPERATURE.

As discussed in the main manuscript, a single parameter scaling function can be written down for the resistance tensor for plateau-to-plateau transitions [15, 24, 25]:

$$R_{xy}(\nu, T) = R_{xy}(\nu_c) f[T^{-\kappa}(\nu - \nu_c)] \tag{S2}$$

This immediately leads to

$$\frac{\mathrm{d}R_{xy}}{\mathrm{d}\nu} \propto T^{-\kappa} \tag{S3}$$

and

$$\frac{\mathrm{d}^2R_{xy}}{\mathrm{d}\nu^2} \propto T^{-2\kappa} \tag{S4}$$

Fig. S4 (a) and (b) show plots of $\mathrm{d}^2R_{xy}/\mathrm{d}\nu^2$ as a function of temperature for two different plateau-to-plateau transitions. Fig. S4 (c) shows the variation of the $\mathrm{d}^2R_{xy}/\mathrm{d}\nu^2$ at $\nu = \nu_c$ with temperature

in log-log scale. The slope yields $2\kappa \approx 0.83$, a value matching very closely with the prediction of Eqn. S4.

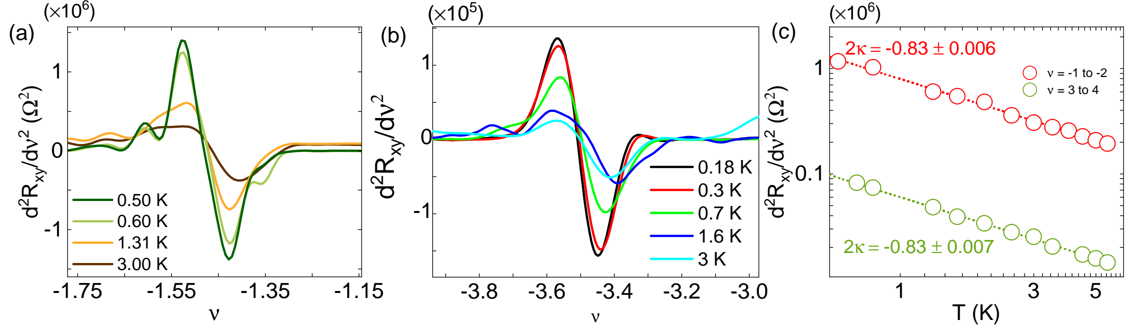

FIG. S4. **Second derivative of R_{xy} with temperature.** Plots of $\mathrm{d}^2R_{xy}/\mathrm{d}\nu^2$ vs ν at different temperatures for plateau-to-plateau transitions between between (a) $\nu = -1$ and $\nu = -2$ and (b) $\nu = -3$ and $\nu = -4$. (c) Log-log plot of $\mathrm{d}^2R_{xy}/\mathrm{d}\nu^2$ vs T for three different PT (open circles). The dotted lines are the linear fits to the data.

S6. FRACTIONAL QUANTUM HALL STATES AT $B = 4.5$ T.

Fig. S5 plots the longitudinal resistance R_{xx} as a function of filling factor ν. We can see the emergence of FQH states at $\nu = N + 1/3$ and $\nu = N + 2/3$ at $B = 4.5$ T.

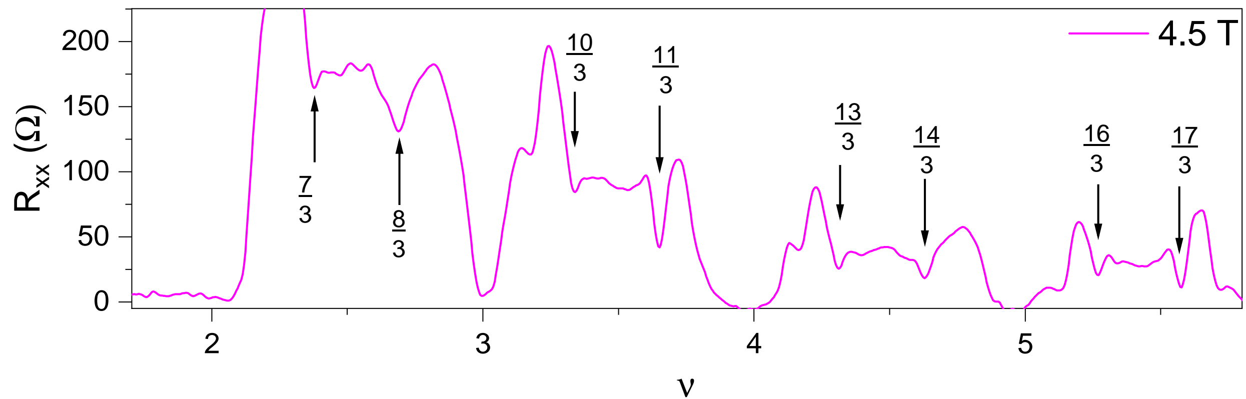

FIG. S5. **Fractional Quantum Hall states at $B = 4.5$ T.** Plot of R_{xx} versus ν measured at $B = 4.5$ T and $T = 20$ mK. The major FQH that begin to form are marked by arrows.

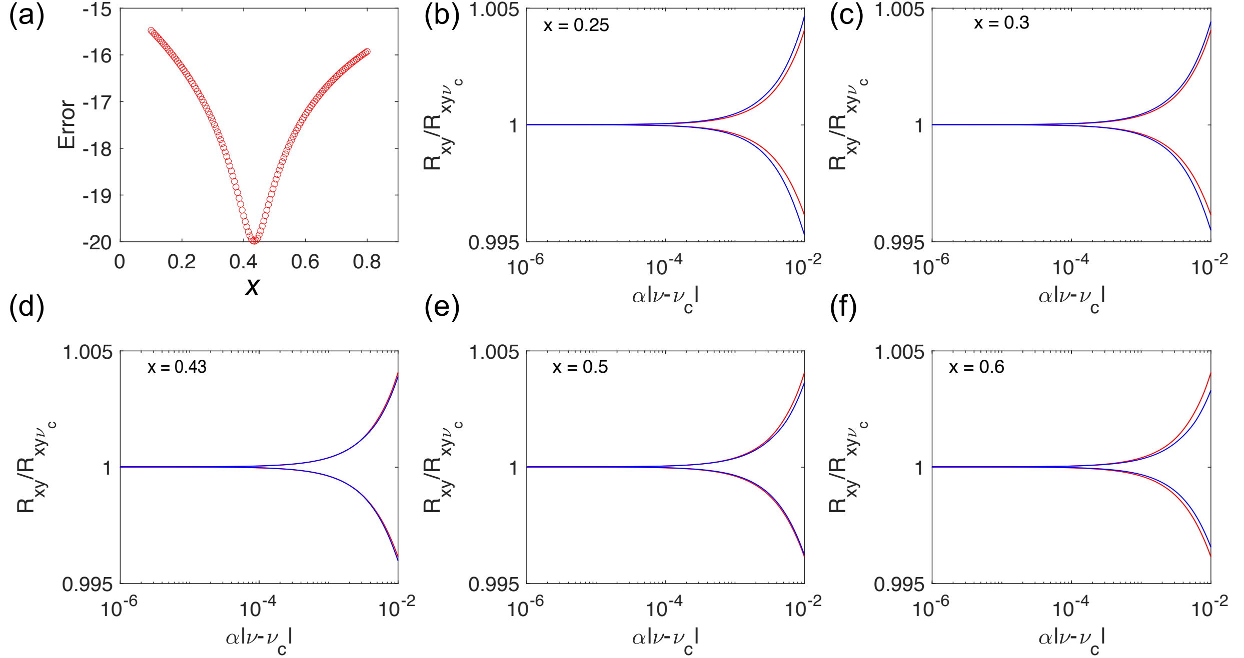

FIG. S6. **Scaling analysis for transition between** $\nu = 2 + 2/3$ **and** $\nu = 2 + 3/5$**.** (a) Plot of the error in scaling versus x. (b-f) Scaling plot for different values of x (the values of x are marked inside the plot).

S7. DETAILS OF SCALING ANALYSIS.

In this section, we describe the process followed to extract the value of κ. As discussed in the main manuscript, we use the following scaling equation [15]:

$$R_{xy}(\nu, T) = R_{xy}(\nu_c) f[\alpha(\nu - \nu_c)] \tag{S5}$$

with

$$\alpha \propto T^{-x} \tag{S6}$$

Fig. S6(b-f) shows $R_{xy}/R_{xy}(\nu_c)$ at various temperatures as a function of $\alpha|\nu - \nu_c|$ for the $\nu = 2 + 2/3$ to $2 + 3/5$ transition. The plots are for different values of x. The red line corresponds to $T = 1.3$ K, and the blue line corresponds to $T = 0.5$ K. For a perfect scaling, these two plots should collapse. However, it is challenging to visually determine the value of x that achieves the best scaling. To address this, the variance between the two plots is calculated as an 'error' metric for the scaling accuracy. We identify κ with the value of x that minimizes this error. In this specific instance, the optimum value is $\kappa = 0.42$, as shown in Fig. S6(a).

S8. VALUES OF κ FROM PREVIOUS STUDIES

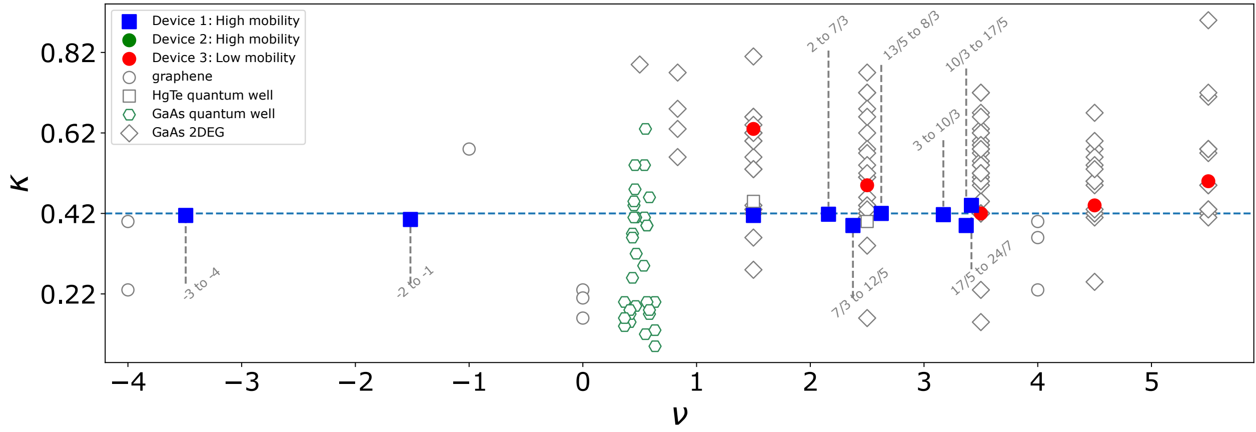

FIG. S7. A compilation of the values of κ from previous studies [26–38], represented by open symbols. The results of the current study are represented with filled squares and circles. Details of the data and the corresponding references are compiled in table S2 and table S3.

TABLE S2: A compilation of the values of κ obtained in 2D materials other than graphene by different groups.

PPT	κ	Material	Reference
1→2/3	0.77±0.02	$Al_xGa_{(1-x)}As - Al_{0:33}Ga_{0:67}As$	[27]
1→2/3	0.63±0.07	$Al_xGa_{(1-x)}As - Al_{0:33}Ga_{0:67}As$	[27]
1→2/3	0.56±0.02	$Al_xGa_{(1-x)}As - Al_{0:33}Ga_{0:67}As$	[27]
1→2/3	0.68±0.05	$Al_xGa_{(1-x)}As - Al_{0:33}Ga_{0:67}As$	[27]
1→2	0.36±0.04	$Al_xGa_{(1-x)}As - Al_{0:33}Ga_{0:67}As$	[27]
1→2	0.56±0.05	$Al_xGa_{(1-x)}As - Al_{0:33}Ga_{0:67}As$	[27]
1→2	0.81±0.04	$Al_xGa_{(1-x)}As - Al_{0:33}Ga_{0:67}As$	[27]
1→2	0.44±0.02	$Al_xGa_{(1-x)}As - Al_{0:33}Ga_{0:67}As$	[27]
1→2	0.53±0.07	$Al_xGa_{(1-x)}As - Al_{0:33}Ga_{0:67}As$	[27]
1→2	0.43±0.10	$Al_xGa_{(1-x)}As - Al_{0:33}Ga_{0:67}As$	[27]
1→2	0.62±0.03	$Al_xGa_{(1-x)}As - Al_{0:33}Ga_{0:67}As$	[27]
1→2	0.28±0.06	$Al_xGa_{(1-x)}As - Al_{0:33}Ga_{0:67}As$	[27]
1→2	0.53±0.06	$Al_xGa_{(1-x)}As - Al_{0:33}Ga_{0:67}As$	[27]
1→2	0.43±0.1	$Al_xGa_{(1-x)}As - Al_{0:33}Ga_{0:67}As$	[27]
2→3	0.51±0.03	$Al_xGa_{(1-x)}As - Al_{0:33}Ga_{0:67}As$	[27]
3→4	0.51±0.03	$Al_xGa_{(1-x)}As - Al_{0:33}Ga_{0:67}As$	[27]
3→4	0.45±0.05	$Al_xGa_{(1-x)}As - Al_{0:33}Ga_{0:67}As$	[27]
3→4	0.45±0.05	$Al_xGa_{(1-x)}As - Al_{0:33}Ga_{0:67}As$	[27]
3→4	0.52±0.03	$Al_xGa_{(1-x)}As - Al_{0:33}Ga_{0:67}As$	[27]
3→4	0.63±0.03	$Al_xGa_{(1-x)}As - Al_{0:33}Ga_{0:67}As$	[27]
1→2	0.42±0.04	$In_{0.53}Ga_{0.47}As/InP$	[26]
2→3, 3→4	0.42±0.04	$In_{0.53}Ga_{0.47}As/InP$	[26]
2→3	0.72±0.05	GaAs/AlGaAs	[39]
4→5	0.15	Si-MOSFET	[39]
3→4	0.25	Si-MOSFET	[39]
5→6	0.15	Si-MOSFET	[39]

2→3,3→4	0.90	Si-MOSFET	[39]
1→2,2→3 3→4	0.62	Si-MOSFET	[39]
6→5	0.71	GaAs/AlGaAs	[40]
7→6	0.72	GaAs/AlGaAs	[40]
6→5	0.74	GaAs/AlGaAs	[40]
7→6	0.77	GaAs/AlGaAs	[40]
8→10	0.75±0.05	GaAs/AlGaAs	[40]
1→2	0.66±0.02	GaAs/AlGaAs	[41]
1→2	0.6±0.02	GaAs/AlGaAs	[41]
1→2	0.62±0.03	GaAs/AlGaAs	[41]
6→5	0.58	$Al_xGa_{1-x}As - Al_{0.33}Ga_{0.67}As(0\%Al)$	[20]
5→4	0.58	$Al_xGa_{1-x}As - Al_{0.33}Ga_{0.67}As(0\%Al)$	[20]
4→3	0.57	$Al_xGa_{1-x}As - Al_{0.33}Ga_{0.67}As(0\%Al)$	[20]
6→5	0.57	$Al_xGa_{1-x}As - Al_{0.33}Ga_{0.67}As(0.21\%Al)$	[20]
5→4	0.56	$Al_xGa_{1-x}As - Al_{0.33}Ga_{0.67}As(0.21\%Al)$	[20]
4→3	0.58	$Al_xGa_{1-x}As - Al_{0.33}Ga_{0.67}As(0.21\%Al)$	[20]
6→5	0.49	$Al_xGa_{1-x}As - Al_{0.33}Ga_{0.67}As(0.33\%Al)$	[20]
5→4	0.5	$Al_xGa_{1-x}As - Al_{0.33}Ga_{0.67}As(0.33\%Al)$	[20]
4→3	0.49	$Al_xGa_{1-x}As - Al_{0.33}Ga_{0.67}As(0.33\%Al)$	[20]
6→5	0.43	$Al_xGa_{1-x}As - Al_{0.33}Ga_{0.67}As(0.85\%Al)$	[20]
5→4	0.42	$Al_xGa_{1-x}As - Al_{0.33}Ga_{0.67}As(0.85\%Al)$	[20]
4→3	0.42	$Al_xGa_{1-x}As - Al_{0.33}Ga_{0.67}As(0.85\%Al)$	[20]
3→2	0.41	$Al_xGa_{1-x}As - Al_{0.33}Ga_{0.67}As(0.85\%Al)$	[20]
6→5	0.42	$Al_xGa_{1-x}As - Al_{0.33}Ga_{0.67}As(0.85\%Al)$	[20]
5→4	0.41	$Al_xGa_{1-x}As - Al_{0.33}Ga_{0.67}As(0.85\%Al)$	[20]
4→3	0.42	$Al_xGa_{1-x}As - Al_{0.33}Ga_{0.67}As(0.85\%Al)$	[20]
3→2	0.42	$Al_xGa_{1-x}As - Al_{0.33}Ga_{0.67}As(0.85\%Al)$	[20]
6→5	0.42	$Al_xGa_{1-x}As - Al_{0.33}Ga_{0.67}As(0.85\%Al)$	[20]

5→4	0.42	$Al_xGa_{1-x}As - Al_{0.33}Ga_{0.67}As$(0.85%Al)	[20]
4→3	0.42	$Al_xGa_{1-x}As - Al_{0.33}Ga_{0.67}As$(0.85%Al)	[20]
3→2	0.41	$Al_xGa_{1-x}As - Al_{0.33}Ga_{0.67}As$(0.85%Al)	[20]
6→5	0.41	$Al_xGa_{1-x}As - Al_{0.33}Ga_{0.67}As$(0.85%Al)	[20]
5→4	0.42	$Al_xGa_{1-x}As - Al_{0.33}Ga_{0.67}As$(0.85%Al)	[20]
4→3	0.42	$Al_xGa_{1-x}As - Al_{0.33}Ga_{0.67}As$(0.85%Al)	[20]
3→2	0.42	$Al_xGa_{1-x}As - Al_{0.33}Ga_{0.67}As$(0.85%Al)	[20]
6→5	0.43	$Al_xGa_{1-x}As - Al_{0.33}Ga_{0.67}As$(1.4%Al)	[20]
5→4	0.43	$Al_xGa_{1-x}As - Al_{0.33}Ga_{0.67}As$(1.4%Al)	[20]
4→3	0.42	$Al_xGa_{1-x}As - Al_{0.33}Ga_{0.67}As$(1.4%Al)	[20]
3→2	0.42	$Al_xGa_{1-x}As - Al_{0.33}Ga_{0.67}As$(1.4%Al)	[20]
6→5	0.49	$Al_xGa_{1-x}As - Al_{0.33}Ga_{0.67}As$(1.9%Al)	[20]
5→4	0.49	$Al_xGa_{1-x}As - Al_{0.33}Ga_{0.67}As$(1.9%Al)	[20]
4→3	0.5	$Al_xGa_{1-x}As - Al_{0.33}Ga_{0.67}As$(1.9%Al)	[20]
3→2	0.51	$Al_xGa_{1-x}As - Al_{0.33}Ga_{0.67}As$(1.9%Al)	[20]
6→5	0.58	$Al_xGa_{1-x}As - Al_{0.33}Ga_{0.67}As$(2.6%Al)	[20]
5→4	0.6	$Al_xGa_{1-x}As - Al_{0.33}Ga_{0.67}As$(2.6%Al)	[20]
4→3	0.59	$Al_xGa_{1-x}As - Al_{0.33}Ga_{0.67}As$(2.6%Al)	[20]
3→2	0.58	$Al_xGa_{1-x}As - Al_{0.33}Ga_{0.67}As$(2.6%Al)	[20]
4→3	0.58	$Al_xGa_{1-x}As - Al_{0.33}Ga_{0.67}As$(4.1%Al)	[20]
3→2	0.57	$Al_xGa_{1-x}As - Al_{0.33}Ga_{0.67}As$ (4.1%Al)	[20]
4→3	0.42±0.01	GaAs/AlGaAs	[16]
4→3	0.67±0.02	GaAs/AlGaAs	[16]
4→3	0.55±0.04	GaAs/AlGaAs	[16]
4→3	0.54±0.02	GaAs/AlGaAs	[16]
4→3	0.23±0.02	GaAs/AlGaAs	[16]
4→3	0.66±0.03	GaAs/AlGaAs	[16]
4→3	0.60±0.02	GaAs/AlGaAs	[16]
4→3	0.54±0.02	GaAs/AlGaAs	[16]

3→2	0.41±0.01	GaAs/AlGaAs	[16]
3→2	0.44±0.02	GaAs/AlGaAs	[16]
3→2	0.46±0.02	GaAs/AlGaAs	[16]
3→2	0.34±0.01	GaAs/AlGaAs	[16]
3→2	0.44±0.02	GaAs/AlGaAs	[16]
3→2	0.42±0.03	GaAs/AlGaAs	[16]
3→2	0.43±0.03	GaAs/AlGaAs	[16]
3→2	0.16±0.02	GaAs/AlGaAs	[16]
2/3→3/5	0.09	GaAs quantum wells (50nm)	[23]
3/5→4/7	0.46	GaAs quantum wells (50nm)	[23]
4/7→5/9	0.39	GaAs quantum wells (50nm)	[23]
6/11→5/9	0.41	GaAs quantum wells (50nm)	[23]
7/13→8/15	0.29	GaAs quantum wells (50nm)	[23]
7/15→6/13	0.19	GaAs quantum wells (50nm)	[23]
6/13→5/11	0.48	GaAs quantum wells (50nm)	[23]
5/11→4/9	0.44	GaAs quantum wells (50nm)	[23]
4/9→3/7	0.37	GaAs quantum wells (50nm)	[23]
3/7→2/5	0.15	GaAs quantum wells (50nm)	[23]
2/5→1/3	0.14	GaAs quantum wells (50nm)	[23]
2/3→3/5	0.20	GaAs quantum wells (30nm)	[23]
3/5→4/7	0.17	GaAs quantum wells (30nm)	[23]
4/7→5/9	0.20	GaAs quantum wells (30nm)	[23]
5/9→6/11	0.63	GaAs quantum wells (30nm)	[23]
6/11→7/13	0.54	GaAs quantum wells (30nm)	[23]
7/15→8/17	0.32	GaAs quantum wells (30nm)	[23]
6/13→7/15	0.41	GaAs quantum wells (30nm)	[23]
6/13→5/11	0.54	GaAs quantum wells (30nm)	[23]
5/11→4/9	0.41	GaAs quantum wells (30nm)	[23]
4/9→3/7	0.26	GaAs quantum wells (30nm)	[23]

3/7→2/5	0.17	GaAs quantum wells (30nm)	[23]
2/5→1/3	0.20	GaAs quantum wells (30nm)	[23]
2/3→3/5	0.13	GaAs quantum wells (40nm)	[23]
3/5→4/7	0.18	GaAs quantum wells (40nm)	[23]
4/7→5/9	0.39	GaAs quantum wells (40nm)	[23]
5/9→6/11	0.12	GaAs quantum wells (40nm)	[23]
5/11→4/9	0.45	GaAs quantum wells (40nm)	[23]
4/9→3/7	0.36	GaAs quantum wells (40nm)	[23]
3/7→2/5	0.18	GaAs quantum wells (40nm)	[23]
2/5→1/3	0.16	GaAs quantum wells (40nm)	[23]
2→1	0.42	GaAs/AlGaAs	[42]
3→4	0.68±0.04	GaAs/AlGaAs	[43]
4→3	0.5 ±0.03	GaAs/AlGaAs	[44]
5→4	0.5±0.03	GaAs/AlGaAs	[44]
4→3	0.62 ±0.04	GaAs/AlGaAs	[45]
4→3	0.59±0.04	GaAs/AlGaAs	[45]
2→1	0.66±0.02	GaAs/AlGaAs	[41]
2→1	0.60±0.0	GaAs/AlGaAs	[41]
2→1	0.62±0.02	GaAs/AlGaAs	[41]
2→1	0.64 ±0.09	GaAs/AlGaAs	[46]
3→4	0.66 - 0.77	GaAs/AlGaAs	[47]
1→0	0.79	GaAs/AlGaAs	[48]
3→2	0.54	GaAs/AlGaAs	[48]
4→3	0.42	GaAs/AlGaAs	[49]
4→3	0.58	GaAs/AlGaAs	[49]
3→2	0.52±0.01	GaAs/AlGaAs	[50]
4→3	0.52±0.02	GaAs/AlGaAs	[50]
5→4	0.53±0.02	GaAs/AlGaAs	[50]
1→2	0.45±0.04	HgTe Quantum wells (5.9 nm)	[51]

2→3	0.40±0.02	HgTe Quantum wells (5.9 nm)	[51]

TABLE S3: Values of κ obtained in graphene from previous studies. The results of our present study are also included.

PPT	κ	Material	Reference
$2 \rightarrow 6$	0.23±0.02	Graphene on SiO_2	[52]
$-2 \rightarrow -6$	0.23±0.02	Graphene on SiO_2	[52]
$-10 \rightarrow -6$	0.23±0.02	Graphene on SiO_2	[52]
$10 \rightarrow 6$	0.23±0.02	Graphene on SiO_2	[52]
$-2 \rightarrow 2$	0.23±0.02	Graphene on SiO_2	[52]
$6 \rightarrow 10$	0.40±0.04	Graphene on SiO_2	[29]
$2 \rightarrow 6$	0.40±0.04	Graphene on SiO_2	[29]
$-2 \rightarrow -6$	0.40±0.03	Graphene on SiO_2	[29]
$-6 \rightarrow -10$	0.40±0.03	Graphene on SiO_2	[29]
$6 \rightarrow 10$	0.41±0.03	Graphene on SiO_2	[29]
$-2 \rightarrow 2$	0.16±0.05	Graphene on SiO_2 Corbino geometry	[32]
$-2 \rightarrow 0$	0.58 ± 0.03	Graphene on SiO_2 (hall bar)	[53]
$-2 \rightarrow 2$	0.21±0.01	Graphene (pnp junction)	[33]
$2 \rightarrow 6$	0.36±0.01	Graphene (pnp junction)	[33]
$6 \rightarrow 10$	0.35±0.01	Graphene (pnp junction)	[33]
$16 \rightarrow 12$	0.27±0.01	Encapsulated BLG	[36]
$12 \rightarrow 8$	0.32±0.01	Encapsulated BLG	[36]
$16 \rightarrow 12$	0.30±0.01	Encapsulated BLG	[36]
$12 \rightarrow 8$	0.32±0.01	Encapsulated BLG	[36]
$-8 \rightarrow -4$	0.30±0.02	Encapsulated BLG	[36]
$-8 \rightarrow -4$	0.29±0.02	Encapsulated BLG	[36]
$-16 \rightarrow -12$	0.32±0.02	Encapsulated BLG	[36]
$-4 \rightarrow -3$	0.41±0.006	Current study (high mobility)	current study
$-2 \rightarrow -1$	0.40±0.005	Current study (high mobility)	current study
$2 \rightarrow 7/3$	0.42±0.004	Current study (high mobility)	current study
$7/3 \rightarrow 12/5$	0.38±0.02	Current study (high mobility)	current study
$10/3 \rightarrow 17/5$	0.39±0.03	Current study (high mobility)	current study

13/5→8/3	0.42±0.01	Current study (high mobility)	current study
3→10/3	0.42±0.009	Current study (high mobility)	current study
17/5→24/7	0.44±0.02	Current study (high mobility)	current study
1→2	0.41±0.007	Current study (high mobility)	current study
1→2	0.63±0.006	Current study (low mobility)	current study
2→3	0.49±0.01	Current study (low mobility)	current study
3→4	0.42±0.009	Current study (low mobility)	current study
4→5	0.44±0.01	Current study (low mobility)	current study
5→6	0.50±0.009	Current study (low mobility)	current study

[1] C. Cong, T. Yu, K. Sato, J. Shang, R. Saito, G. F. Dresselhaus, and M. S. Dresselhaus, ACS Nano **5**, 8760 (2011), https://doi.org/10.1021/nn203472f.

[2] T. A. Nguyen, J.-U. Lee, D. Yoon, and H. Cheong, Scientific reports **4**, 4630 (2014).

[3] L. Wang, I. Meric, P. Y. Huang, Q. Gao, Y. Gao, H. Tran, T. Taniguchi, K. Watanabe, L. M. Campos, D. A. Muller, J. Guo, P. Kim, J. Hone, K. L. Shepard, and C. R. Dean, Science **342**, 614 (2013), http://science.sciencemag.org/content/342/6158/614.full.pdf.

[4] P. Tiwari, S. P. Srivastav, and A. Bid, Phys. Rev. Lett. **126**, 096801 (2021).

[5] C. H. Lui, Z. Li, K. F. Mak, E. Cappelluti, and T. F. Heinz, Nature Physics **7**, 944 (2011).

[6] Y.-P. Wang, X.-G. Li, J. N. Fry, and H.-P. Cheng, Physical Review B **94**, 165428 (2016).

[7] B. Datta, H. Agarwal, A. Samanta, A. Ratnakar, K. Watanabe, T. Taniguchi, R. Sensarma, and M. M. Deshmukh, Physical Review Letters **121**, 056801 (2018).

[8] G. Chen, L. Jiang, S. Wu, B. Lyu, H. Li, B. L. Chittari, K. Watanabe, T. Taniguchi, Z. Shi, J. Jung, *et al.*, Nature Physics **15**, 237 (2019).

[9] H. Zhou, T. Xie, T. Taniguchi, K. Watanabe, and A. F. Young, Nature **598**, 434 (2021).

[10] K. Zou, F. Zhang, C. Clapp, A. MacDonald, and J. Zhu, Nano letters **13**, 369 (2013).

[11] S. H. Jhang, M. F. Craciun, S. Schmidmeier, S. Tokumitsu, S. Russo, M. Yamamoto, Y. Skourski, J. Wosnitza, S. Tarucha, J. Eroms, and C. Strunk, Physical Review B **84**, 161408 (2011).

[12] D. G. Polyakov and B. I. Shklovskii, Phys. Rev. Lett. **70**, 3796 (1993).

[13] P. Stepanov, Y. Barlas, T. Espiritu, S. Che, K. Watanabe, T. Taniguchi, D. Smirnov, and C. N. Lau, Phys. Rev. Lett. **117**, 076807 (2016).

[14] T. Taychatanapat, K. Watanabe, T. Taniguchi, and P. Jarillo-Herrero, Nature Physics **7**, 621 (2011).

[15] B. Huckestein, Rev. Mod. Phys. **67**, 357 (1995).

[16] N. A. Dodoo-Amoo, K. Saeed, D. Mistry, S. P. Khanna, L. Li, E. H. Linfield, A. G. Davies, and J. E. Cunningham, Journal of Physics: Condensed Matter **26**, 475801 (2014).

[17] L. Engel, H. Wei, D. Tsui, and M. Shayegan, Surface science **229**, 13 (1990).

[18] V. Goldman, J. K. Jain, and M. Shayegan, Phys. Rev. Lett. **65**, 907 (1990).

[19] S. Pu, G. J. Sreejith, and J. K. Jain, Phys. Rev. Lett. **128**, 116801 (2022).

[20] W. Li, G. A. Csáthy, D. C. Tsui, L. N. Pfeiffer, and K. W. West, Phys. Rev. Lett. **94**, 206807 (2005).

[21] J. Martin, N. Akerman, G. Ulbricht, T. Lohmann, J. H. Smet, K. von Klitzing, and A. Yacoby, Nature Physics **4**, 144 (2008).

[22] S. Sarkar, K. R. Amin, R. Modak, A. Singh, S. Mukerjee, and A. Bid, Scientific Reports **5**, 16772 (2015).

[23] P. T. Madathil, K. A. Villegas Rosales, C. T. Tai, Y. J. Chung, L. N. Pfeiffer, K. W. West, K. W. Baldwin, and M. Shayegan, Phys. Rev. Lett. **130**, 226503 (2023).

[24] A. Pruisken, Physical review letters **61**, 1297 (1988).

[25] H. Wei, S. Hwang, D. Tsui, and A. Pruisken, Surface Science **229**, 34 (1990).

[26] H. P. Wei, D. C. Tsui, M. A. Paalanen, and A. M. M. Pruisken, Phys. Rev. Lett. **61**, 1294 (1988).

[27] S. Koch, R. J. Haug, K. v. Klitzing, and K. Ploog, Phys. Rev. B **43**, 6828 (1991).

[28] W. Li, C. L. Vicente, J. S. Xia, W. Pan, D. C. Tsui, L. N. Pfeiffer, and K. W. West, Phys. Rev. Lett. **102**, 216801 (2009).

[29] A. J. M. Giesbers, U. Zeitler, L. A. Ponomarenko, R. Yang, K. S. Novoselov, A. K. Geim, and J. C. Maan, Phys. Rev. B **80**, 241411 (2009).

[30] T. Shen, A. T. Neal, M. L. Bolen, J. J. Gu, L. W. Engel, M. A. Capano, and P. D. Ye, Journal of Applied Physics **111**, 013716 (2012).

[31] E. Pallecchi, M. Ridene, D. Kazazis, F. Lafont, F. Schopfer, W. Poirier, M. O. Goerbig, D. Mailly, and A. Ouerghi, Scientific Reports **3**, 1791 (2013).

[32] E. C. Peters, A. J. M. Giesbers, M. Burghard, and K. Kern, Appl. Phys. Lett. **104**, 203109 (2014).

[33] C.-H. Liu, P.-H. Wang, T.-P. Woo, F.-Y. Shih, S.-C. Liou, P.-H. Ho, C.-W. Chen, C.-T. Liang, and W.-H. Wang, Phys. Rev. B **93**, 041421 (2016).

[34] M. Amado, E. Diez, F. Rossella, V. Bellani, D. Lopez-Romero, and D. K. Maude, Journal of Physics: Condensed Matter **24**, 305302 (2012).

[35] B. Jabakhanji, A. Michon, C. Consejo, W. Desrat, M. Portail, A. Tiberj, M. Paillet, A. Zahab, F. Cheynis, F. Lafont, F. Schopfer, W. Poirier, F. Bertran, P. Le Févre, A. Taleb-Ibrahimi, D. Kazazis, W. Escoffier, B. C. Camargo, Y. Kopelevich, J. Camassel, and B. Jouault, Phys. Rev. B **89**, 085422 (2014).

[36] C. Cobaleda, S. Pezzini, A. Rodriguez, E. Diez, and V. Bellani, Phys. Rev. B **90**, 161408 (2014).

[37] E. J. Dresselhaus, B. Sbierski, and I. A. Gruzberg, Annals of Physics **435**, 168676 (2021), special Issue on Localisation 2020.

[38] M. R. Zirnbauer, Nuclear Physics B **941**, 458 (2019).

[39] S. Koch, R. J. Haug, K. v. Klitzing, and K. Ploog, Phys. Rev. B **46**, 1596 (1992).

[40] Y. J. Zhao, T. Tu, X. J. Hao, G. C. Guo, H. W. Jiang, and G. P. Guo, Phys. Rev. B **78**, 233301 (2008).

[41] F. Hohls, U. Zeitler, and R. J. Haug, Phys. Rev. Lett. **88**, 036802 (2002).

[42] H. P. Wei, S. Y. Lin, D. C. Tsui, and A. M. M. Pruisken, Phys. Rev. B **45**, 3926 (1992).

[43] S. Koch, R. J. Haug, K. v. Klitzing, and K. Ploog, Phys. Rev. Lett. **67**, 883 (1991).

[44] K.-H. Yoo, H. Kwon, and J. Park, Solid State Communications **92**, 821 (1994).

[45] S. Koch, R. J. Haug, K. von Klitzing, and K. Ploog, Semiconductor Science and Technology **10**, 209 (1995).

[46] C. Huang, Y. Chang, H. Cheng, C.-T. Liang, and G. Hwang, Physica E: Low-dimensional Systems and Nanostructures **22**, 232 (2004), 15th International Conference on Electronic Propreties of Two-Dimensional Systems (EP2DS-15).

[47] T. Tu, Y.-J. Zhao, G.-P. Guo, X.-J. Hao, and G.-C. Guo, Physics Letters A **368**, 108 (2007).

[48] T. Nakajima, T. Ueda, and S. Komiyama, Journal of the Physical Society of Japan **76**, 094703 (2007), https://doi.org/10.1143/JPSJ.76.094703.

[49] W. Li, J. S. Xia, C. Vicente, N. S. Sullivan, W. Pan, D. C. Tsui, L. N. Pfeiffer, and K. W. West, Phys. Rev. B **81**, 033305 (2010).

[50] X. Wang, H. Liu, J. Zhu, P. Shan, P. Wang, H. Fu, L. Du, L. N. Pfeiffer, K. W. West, X. C. Xie, R.-R. Du, and X. Lin, Phys. Rev. B **93**, 075307 (2016).

[51] T. Khouri, M. Bendias, P. Leubner, C. Brüne, H. Buhmann, L. W. Molenkamp, U. Zeitler, N. E. Hussey, and S. Wiedmann, Phys. Rev. B **93**, 125308 (2016).

[52] K. Bennaceur, P. Jacques, F. Portier, P. Roche, and D. C. Glattli, Phys. Rev. B **86**, 085433 (2012).

[53] M. Amado, E. Diez, D. López-Romero, F. Rossella, J. Caridad, F. Dionigi, V. Bellani, and D. Maude, New Journal of Physics **12**, 053004 (2010).